

Theoretical and Experimental Research on Slip and Uplift of the Timber-Concrete Composite Beam

Jianying Chen,^a Guojing He,^{a,*} Xiaodong (Alice) Wang,^b Jiejun Wang,^a JinYi,^a and Chuanjian Yang^a

Timber-concrete composite beams are a new type of structural element that is environmentally friendly. The structural efficiency of this kind of beam highly depends on the stiffness of the interlayer connection. The structural efficiency of the composite was evaluated by experimental and theoretical investigations performed on the relative horizontal slip and vertical uplift along the interlayer between composite's timber and concrete slab. Differential equations were established based on a theoretical analysis of combination effects of interlayer slip and vertical uplift, by using deformation theory of elastics. Subsequently, the differential equations were solved and the magnitude of uplift force at the interlayer was obtained. It was concluded that the theoretical calculations were in good agreement with the results of experimentation.

Keywords: Timber-concrete composite beam; Interlayer slip; Vertical uplift; bolt; Differential equations

Contact information: a: College of Civil Engineering, Central South University of Forestry and Technology, 498 Shaoshan Road, Changsha, Hunan, 410004 China; b: Department of Wood and Forest Sciences, Pavillon Kruger, Laval University, Quebec, Q. C., Canada G1V 0A6;

* Corresponding author: znykj498cgy@hotmail.com; cegjhe@hotmail.com; cgy801123@126.com

INTRODUCTION

The timber-concrete composite (TCC) structure is a construction technique in which a timber beam is connected to an upper concrete slab using different types of connectors. The advantages of the different materials properties can be utilized, where bending and tensile forces get primarily resisted by the timber, whereas the compression force is resisted by the concrete topping (Gutkowski *et al.* 2008). The structural efficiency of a TCC highly depends on the stiffness of the interlayer connection (Yeho *et al.* 2011), where shear deformation and axial deformation of a flexible shear connector, such as a bolt, leads to an inevitable interlayer slip and vertical uplift between the timber beam and the concrete slab. This action reduces the combination effect and stiffness of the composite-beam section, resulting in decreased bending-loading capacity and increased deformation of the composite beam (Rodrigues *et al.* 2013). Studies of the interlayer slip, vertical-uplift pattern, and their influence on the ultimate loading capacity and deformation of the composite beam structure are therefore needed.

Previous studies aimed at describing this composite structure have analyzed the relative horizontal slip caused by longitudinal shearing along the interlayer between timber beams and the concrete slab by use of various numerical methods, including finite element methods (Ayoub 2001, 2005; Ranzi *et al.* 2004; Cas *et al.* 2004; EN1995-2 2004; Jorge *et al.* 2010; Dias *et al.* 2011, 2012, 2015; Lopes *et al.* 2012; Martins *et al.* 2016; Cas *et al.* 2018). However, investigations of the vertical-uplift force between timber beams and the concrete slab are rare. The finite element model of the composite beam proposed by Gara *et al.* (2006) was the only model that considered longitudinal slip and vertical uplift. In the

British codes (BS5400-5, 2005), the shear resistance of the connector in composite beams and its vertical-uplift force must be computed. However, the method of the calculation is not specified in the code.

The objective of this study was to research the influence on the interface slip and vertical lifting force by changing the shear connection ratios and the arrangement of the bolts. The specific objective was to calculate the vertical-uplift force and develop differential equations of simply supported TCC beams with respect to the interface slip and vertical uplift.

EXPERIMENTAL

Specimens and Material Properties

The experimental tests investigated the influence of different shear connection ratios and arrangement of shear connectors on relative horizontal slip and vertical-uplift force. The bolt connector is assumed to act as a tension member of the vertical-uplift force in the experiment. Additionally, the uplift of the composite beam is assumed to be small, and the axial tensile stress of the bolt cannot reach the tensile yield strength. The strain gauges were attached to each side of the middle section of the bolt rod and perpendicular to the longitudinal direction of the beam. The experimental magnitude of the uplift force on the bolt can be calculated based on the measured strain under load and the bolt properties, as shown in Eq. 1.

$$F = E_s \cdot \varepsilon_s \cdot A_s \quad (1)$$

In this equation, F is the vertical-uplift force, E_s is the elastic modulus of the bolt, ε_s is the average strain of the two sides of the bolt, and A_s is the cross-sectional area of the bolt.

Five simply supported 2.8 m span TCC beams with bolt connectors were constructed for the experiment. To enhance the overall performance of composite beams, the concrete slabs were configured with longitudinal and horizontal steel bars with yield strength of 330 MPa. The diameter of these steel bars was 8 mm, and the spacing was 100 mm. By changing the shear connection ratios of connection and arrangement of the bolts, this work studied the influence of interface slip and vertical lifting force. The parameters of each specimen are shown in Table 1, and the construction process of the beams is shown in Fig. 1.



Fig. 1. Construction of the TCC

The structural efficiency of a TCC beam highly depends on the number of shear connectors. In this study, the shear connection ratios of composite beams was evaluated in terms of the ratio of the number of shear connectors (n) used in the composite beam, to the number of shear connectors used in the composite beam with a full shear connection (n_f), *i.e.* (n/n_f). The number of shear connectors used in the composite beam with a full shear connection (n_f) can be calculated using Eq. 2,

$$n_f = V_1/N_f \quad (2)$$

where V_1 is the maximum longitudinal shear force at the interface and N_f is the shear bearing capacity of an individual connector with a theoretical value of 26.6 kN (He *et al.* 2016).

Table 1. Timber-Concrete Composite Beam Specimen Parameters

NO. of Beam	Dimension of beam	Dimension of slab	Bolt spacing (mm)		Shear connection ratios of connection
	Height × Width (mm)	Height × Width (mm)	Bend-shear stage	Pure bending stage	
CWW1	300 × 100	70 × 400	100	100	1
CWW2	300 × 100	70 × 400	140	140	0.72
CWW3	300 × 100	70 × 400	200	200	0.52
CWW4	300 × 100	70 × 400	280	280	0.38
CWW5	300 × 100	70 × 400	123	290	0.72

Timber

The glued timber blocks used in the tests were made of Xing'an larch wood and joined with polyurethane glue. Six specimens were tested according to the in the test method for tensile strength parallel to grain of wood (GB/T 1938-2009) (Fig. 2), where the tensile strength was found to be 115.9 MPa. According to the method of testing in compressive strength parallel to grain of wood (GB/T 1935-2009), six full scale specimens with dimensions of 30 mm x20 mm x 20 mm were tested (Fig. 3), where the compressive strength was 48.2 MPa. The modulus of elasticity in compression parallel to grain of wood (GB/T 15777-2017) was tested for seven full scale specimens with dimensions of 60 mm × 20 mm × 20 mm were tested (Fig. 4), and the modulus of elasticity was 13.8 GPa.

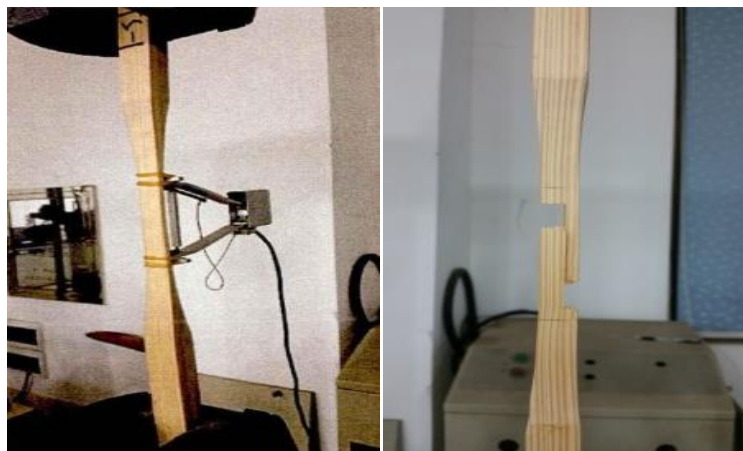


Fig. 2. Tensile strength test of timber



Fig. 3. Compressive strength test of timber



Fig. 4. Test for the modulus of elasticity in compression parallel to grain of wood

The density of the timber was determined for six wood pieces with the dimension 20 mm × 20 mm × 20 mm. The mean density of the timber was found to be 552.0 kg/m³.

Concrete

Six concrete blocks with a size of 150 mm×150 mm×150mm were made in the laboratory of Central South University of Forestry and Technology, where also the five TCC slabs were cast. The expected strength class of the concrete was C30. The actual mean strength of the concrete was 31.78 MPa, and the actual mean density of concrete was found to be 2385.0 kg/m³ (Fig. 5). The elastic modulus of the concrete was 30 GPa.

The high-strength bolts were of diameter 16 mm and length 120 mm, had M-threading and were bought from Suzhou Qiangda Fastener Industry Co., Suzhou, China. The material parameters were provided by the manufacturer, where the bolt tensile strength was 1200 MPa with yield strength of 1080 MPa. The elastic modulus of the bolt was 210 GPa. In this paper, the bolt-penetration depth in the timber was 80 mm.

Base on the following Eq. 3, the horizontal shear stiffness (K_1) of the bolts in the positive moment region was calculated to be 7862 N/mm by using the experimental properties of the concrete and bolts.

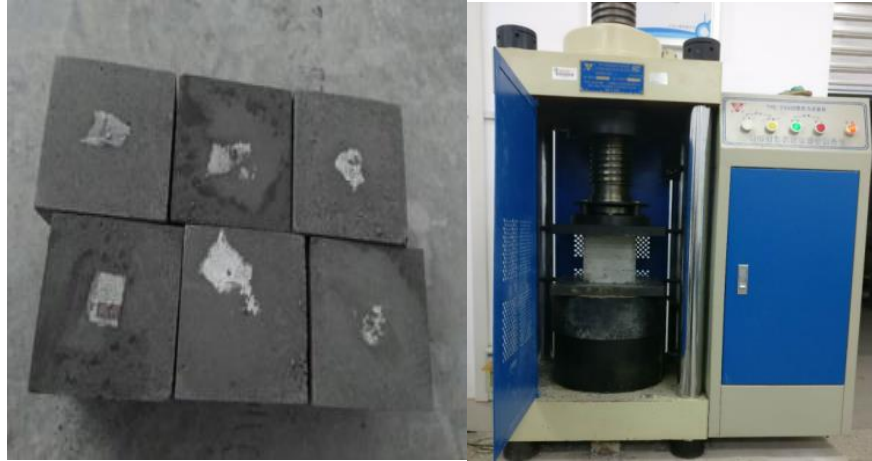


Fig. 5. Compressive strength test of concrete

Test Device and Procedure

In this test, the bending load was applied with a distribution beam at a 2-point symmetric section. The load was applied by a 20-ton mechanical jack, and the loading speed was controlled by an ancillary reader and force sensor. A steel backing plate was placed at each loading point to avoid stress concentrations leading to local crushing of the concrete. The test is a static monotonic loading test, divided into a preloading phase and a loading phase. The preloading phase was completed in three stages with a loading of 8 kN per stage. Data acquisitions of the preload phase were performed to verify that the data was reasonable and that each device functioned normally. The loading phase also applied a loading of 8 kN per stage. Near the cracking load, the loading was reduced to 4 kN per stage. The beam was allowed to rest for approximately 2 min after each loading to allow the deformation of the beam to be fully formed. The data were collected with a static strain tester (TST38326, Jingjiang Tester Co., Ltd., Jingjiang, China), and the location and developing trend of the crack was monitored.

The strains of the timber beam and the concrete slab were measured by electric resistance strain gauges. The timber beam deflection, the relative horizontal slip between the timber beam and concrete slab, and the vertical-uplift displacement between the timber beam and the concrete slab were measured with dial indicators (321-123-4D, Guilin Guanglu Digital Measurement and Control Co., Ltd., Guilin, China). The on-site test-loading apparatus of the composite beam is shown in Fig. 6.

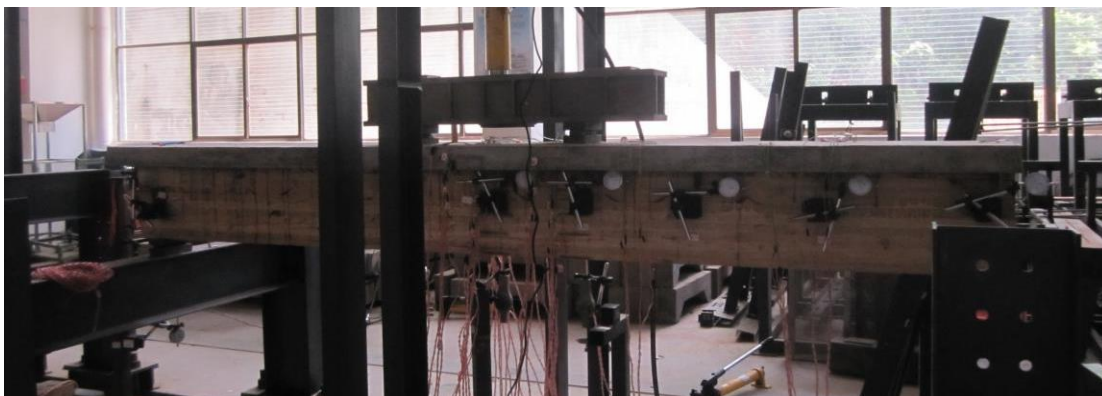


Fig. 6. Photo of the TCC beam loading experiment

Experimental Description

Five composite beams with a large shear span ratio were designed for the bending test. All specimens failed in bending mode; even if partial shear connectors were used, there was no shear failure of the bolt. The specific failure process of each specimen was similar; *i.e.*, when the load reached approximately 0.1 P_u (P_u is the ultimate bearing capacity of the composite beam), the natural bonding of the interlayer along the concrete slab and the timber beam began to fail. When the load reached approximately 0.4 P_u , the engineered timber beam emitted a subtle sound and the concrete slab showed visible bending cracks on the base edge of the loading point. When the load reached approximately 0.6 P_u , the engineering timber beam made a loud snapping sound, the timber fibre on the lower edge of the timber beam began to fail, and the concrete slab showed visible bending cracks on the edge of the loading point. The bending cracks increased in number and expanded as the load was increased. When the load reached P_u (P_u of CWW1, CWW2 and CWW3 were 176KN, 168KN and 152KN respectively), the upper edge of the concrete slab was crushed at the loading point, the lower edge of the concrete slab was tensile-fractured, and the base edge of the timber beam was tensile-fractured, resulting in a loss of bearing capacity of the composite beam. Because the bonding layer in the beams CWW4 and CWW5 had insufficient strength, the cementing layers cracked prior to overall failure of the beam because of insufficient shear strength, which led to a loss of bearing capacity and an early failure of the composite beam. Failure was shown to occur when beam CWW4 was loaded to 100 kN and beam CWW5 was loaded to 132 kN.

Analysis of Test Results

The magnitude of relative horizontal slip and vertical-uplift displacement along the interlayer of the composite beam are the key factors that reflect the structural efficiency of a TCC beam. Figure 7 shows the displacement gauge diagram of the slip and uplift measurements for the TCC beam. In Fig. 7, N1-N4 are the displacement gauges that measured the relative horizontal slip: from the midspan to the end of the beam, while N5 and N6 are the displacement gauges that measured the uplift on both ends.

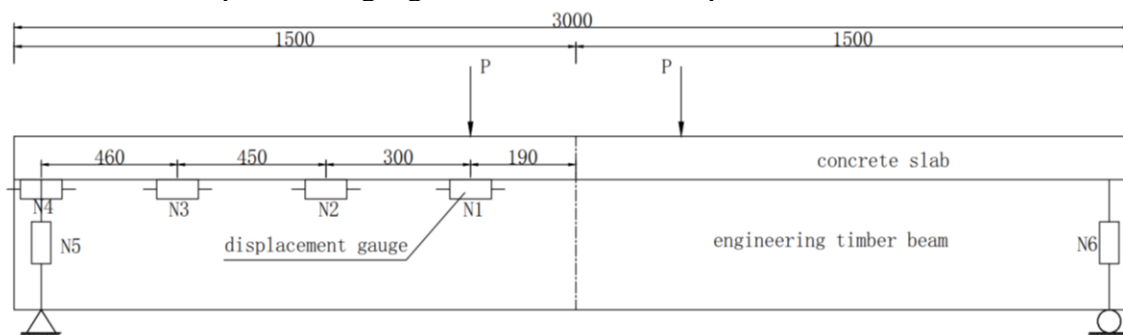


Fig. 7. Displacement gauge diagram of the slip and uplift measurement

In Fig. 8, the relative horizontal slip curve of the tested composite beam is shown. The uplift displacement curve of the tested composite beam is shown in Fig. 9. The characteristics of the composite beam in relative horizontal slip and vertical uplift lead to the following conclusions:

(1) The spacing of the bolt, *i.e.*, the shear connection ratios of the shear connectors has a significant influence on the relative horizontal slip of the interlayer. The relative horizontal slip increases as the spacing between two adjacent bolt connectors increases.

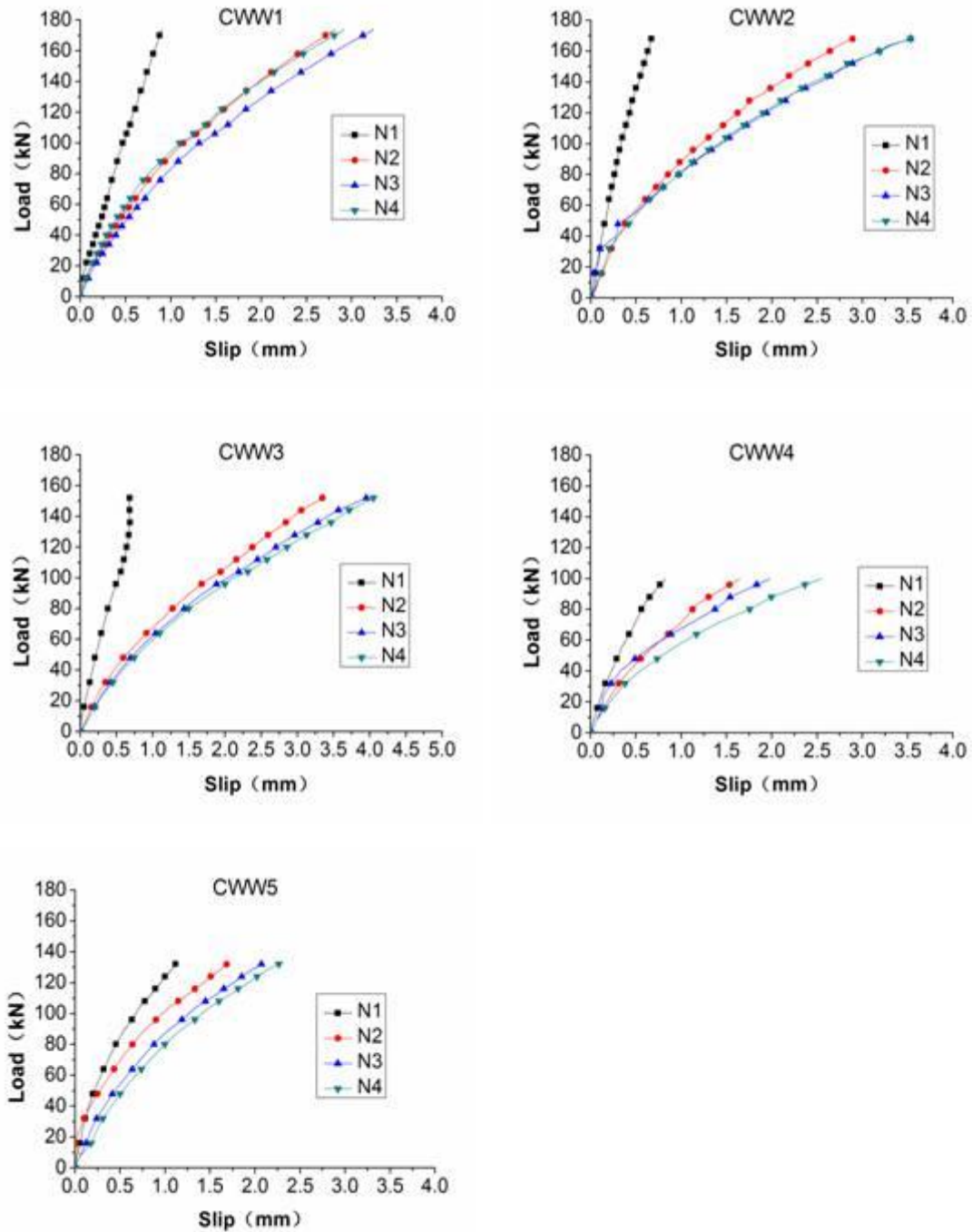


Fig. 8. Measured slip distribution curves of the TCC beam

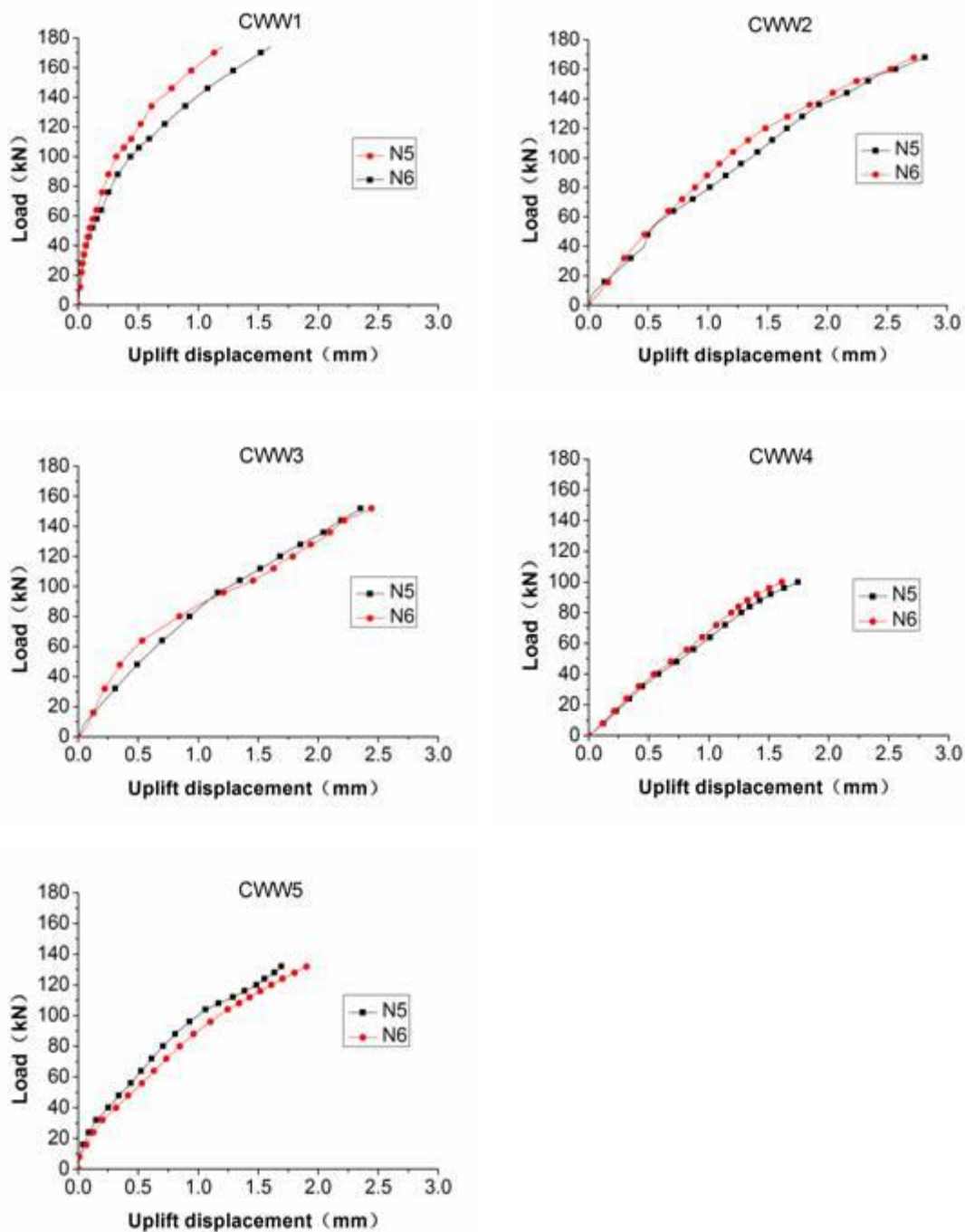


Fig. 9. The measured uplift displacement curves on the beam end of the TCC beam

For beams CWW1 to CWW4, the bolt spacing increases from 100 mm to 280 mm, and the relative horizontal slip on the beam ends increases from 1.3 mm to 2.6 mm under a vertical load of 100 kN.

(2) As the load increases continuously, the value of the relative horizontal slip also increases continuously, and the development rate of the slip at the later loading stage is significantly faster than that of previous stages. The measured results indicate that when the load exceeds $0.1 P_u$, the relative horizontal slip begins to occur at the interlayer between the timber beam and the concrete slab, and as the load increases continuously, the relative horizontal slip also increases. When the load goes over $0.4 P_u$, the development rate of the relative horizontal slip accelerates significantly.

(3) When the bolts are evenly positioned along the beam, the maximum relative horizontal slip occurs near the end of the beam. The relative horizontal slip gradually decreases from the beam end to the midspan and its value is small within a distance of $L/6$ to both sides of the midspan.

(4) The shear connection ratio of the shear connectors is the same for beams CWW2 and CWW5, but their arrangement is different. Under the same load, the uplift displacement is slightly smaller on the end of beam CWW5 than on the end of beam CWW2, indicating that the arrangement of CWW5 is better.

(5) The uplift displacement at the end of the composite beam increases as the spacing between two adjacent bolt connectors increases. When the bolt spacing increases from 100 mm to 280 mm from beam CWW2 to beam CWW4, the uplift displacement increases gradually from 0.6 mm to 1.8 mm under a vertical load of 100 kN.

(6) As the load increases continuously, the vertical-uplift displacement also increases continuously; the development rate of the uplift displacement at later loading stages is gradually increasing compared with that of previous stages.

(7) The slip detected by gauge N4 at the end of beam CWW1 was smaller than that detected by gauge N3. This result is mainly attributed to the full-section compression of the concrete flange because the beam CWW1 was the composite beam with a full shear connection, and the constraints by the support at the end of the beam. By contrast, this phenomenon did not occur in beams with partial shear connections.

THEORETICAL ANALYSIS

Basic Assumptions

Under the operating load, the timber-concrete composite beam approximates an elastic stage. The compressive strain of the concrete slab also lies in the linearly increasing segment of the stress-strain curve. The timber beam and the concrete slab can be viewed as approximate elastic bodies with the following assumptions:

(1) The vertical-uplift force along the interlayer of the composite beam is positively proportional to the relative deflection difference between the top surface of the upper-wing edge of the timber beam and the base of the concrete slab, *i.e.* the uplift displacement.

(2) The horizontal shear force along the interlayer of the composite beam is positively proportional to the relative horizontal displacement difference between the timber beam and the concrete slab, *i.e.*, the magnitude of its relative slip.

(3) Assume that the timber beam and the concrete slab of the composite beam obey the cross-section assumption at loading. Although the bending curvatures vary, each satisfies the basic bending theory.

Stiffness Coefficient

Based on the above assumptions, to calculate the interaction between the TCC

beams along the interlayer, the horizontal shear stiffness and the vertical anti-uplift stiffness of the bolt shear connector must be estimated as follows:

(1) The horizontal shear stiffness K_1 is the horizontal shear per unit slip. The following formula was proposed based on the experimental formulas by He *et al.* (2016), Xie *et al.* (2017), Fu *et al.* (2008), and Jiang *et al.* (2007),

$$K_1 = 0.03\sqrt{E_w \cdot l_w} \cdot d^2 \tag{3}$$

where E_w is the elastic modulus of the timber, d is the bolt-connector diameter, and l_w is the length of the bolt connector embedded in the timber.

(2) Vertical anti-uplift stiffness K_v is the vertical tensile force per unit uplift displacement, which can be calculated based on experimental results and according to the following definition of uplift stiffness,

$$K_v = F/Y \tag{4}$$

where Y is the vertical uplift displacement between the timber beam and the concrete slab at the bolt location.

Model Construction

As shown in Fig.10, an infinitesimal element dx is defined under concentrated loading. The meaning of each variable is listed in Table 2.

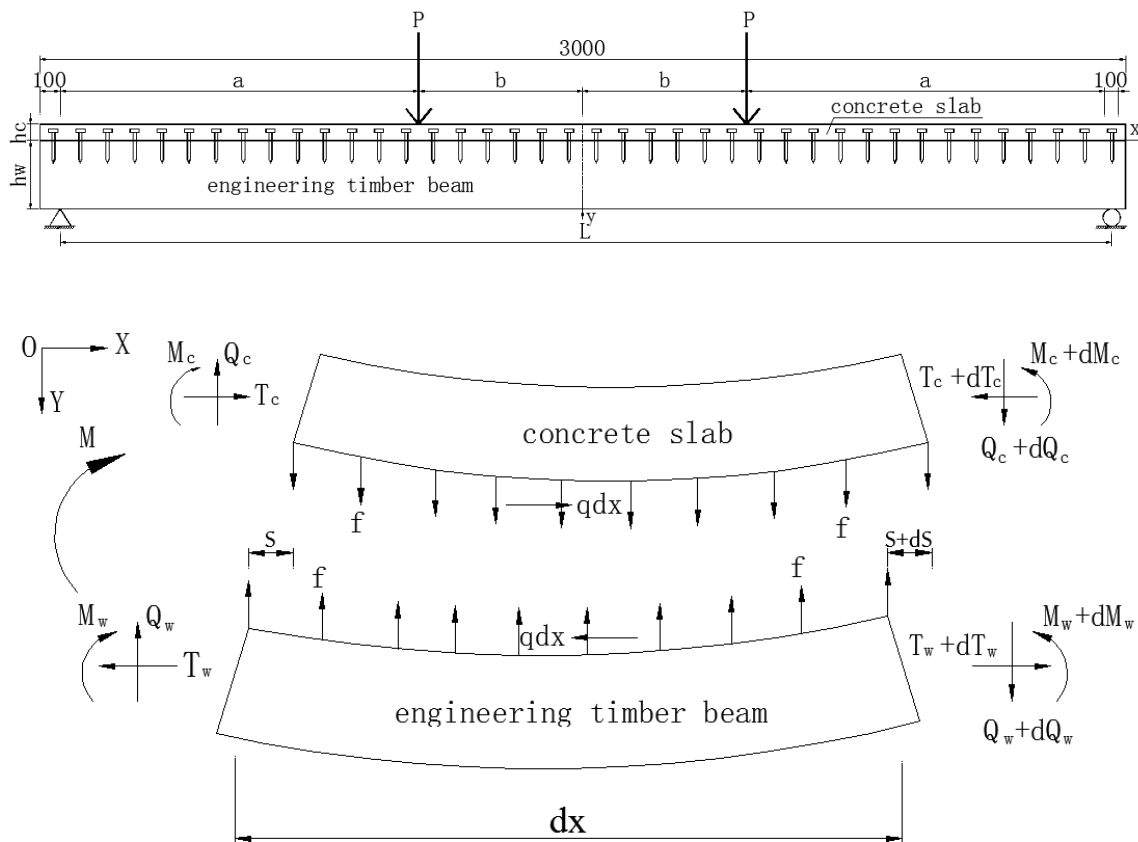


Fig. 10. Infinitesimal element force diagram of the TCC beam

Table 2. Meaning of Each Variable of the TCC Beam

Symbol (units)	Meaning	Symbol (units)	Meaning
L (m)	Composite beam span	F (kN)	Uplift force on bolt
P (kN)	Concentrated load on the composite beam	f (kN/m)	Vertical uplift force per unit length on the interlayer
h_c (m)	Section height of the concrete slab	q (kN/m)	Horizontal shear per unit length on the interlayer
h_w (m)	Section height of the timber beam	S (m)	Relative horizontal slip on the interlayer
h (m)	Distance between the centroidal axis of the two cross-sections of the composite beam	Y (m)	Vertical uplift on the interlayer
T_c (kN)	Axial force of the concrete slab	Q_c (kN)	Vertical shear of the concrete slab
T_w (kN)	Axial force of the timber beam	Q_w (kN)	Vertical shear of the timber beam
M_c (kN·m)	Bending moment by the concrete slab alone	y_c (m)	Vertical deflection of the concrete slab
M_w (kN·m)	Bending moment by the timber beam alone	y_w (m)	Vertical deflection of the timber beam
M (kN·m)	External bending moment by the composite beam		

Development of the Differential Equations

The shear-resistant connector of the bolt is evenly placed in the composite beam with a bolt spacing of e . The following equation can be obtained from Eq. 4:

$$F = e \cdot f = K_v \cdot (y_w - y_c) = K_v \cdot Y \quad (5)$$

Set the tensile strain of the fibre under the concrete slab and the tensile strain of the fibre on the timber beam to ε_w and $d\varepsilon_c$, respectively. The relative horizontal slip increment on the beam segment dx is dS . Using the deformation coordination conditions, the slip strain $\Delta\varepsilon$ is as follows:

$$\Delta\varepsilon = dS/dx = \varepsilon_w - \varepsilon_c \quad (6)$$

If $T_c = T_w = T$, then the strain of the concrete slab and the timber beam is obtained by $\sum x=0$ and $\sum y=0$ as follows:

$$f = -dQ_c/dx \quad (7)$$

$$f = dQ_w/dx \quad (8)$$

$$q = dT/dx \quad (9)$$

Differentiate Eq. 5 as follows:

$$\frac{d^2 f}{dx^2} = \frac{K_v}{e} \cdot \left(\frac{d^2 y_w}{dx^2} - \frac{d^2 y_c}{dx^2} \right) \quad (10)$$

The sectional curvature, the elastic modulus and the moment of inertia of the concrete slab and the timber beam are ϕ_c , ϕ_w , E_c , E_w , I_c , and I_w , respectively. The correlation among the deflection, the bending moment and the curvature results in the following:

$$\emptyset_w = -\frac{d^2 y_w}{dx^2} = \frac{M_w}{E_w \cdot I_w} \quad (11a)$$

$$\emptyset_c = -\frac{d^2 y_c}{dx^2} = \frac{M_c}{E_c \cdot I_c} \quad (11b)$$

Substituting Eqs. 11a and 11b into Eq. 10 and differentiating results in Eq. 12 as follows:

$$\frac{d^4 f}{dx^4} = \frac{K_v}{e} \cdot \left(\frac{1}{E_c \cdot I_c} \frac{d^2 M_c}{dx^2} - \frac{1}{E_w \cdot I_w} \frac{d^2 M_w}{dx^2} \right) \quad (12)$$

In Fig. 10, take the moment on the left cross-section of the infinitesimal element from the concrete slab, omit the high-order differential terms $dQ_c \cdot dx$ and $f \cdot dx^2/2$, and combine the result with Eq. 7 to obtain the following equation:

$$\frac{d^2 M_c}{dx^2} = -f - \frac{h_c}{2} \cdot \frac{dq}{dx} \quad (13)$$

In Fig. 10, take the moment on the left cross-section of the infinitesimal element from the timber beam, omit the high-order differential terms $dQ_w \cdot dx$ and $f \cdot dx^2/2$, then differentiate the result and combine it with Eq. 8 to obtain the following equation:

$$\frac{d^2 M_w}{dx^2} = f - \frac{h_w}{2} \cdot \frac{dq}{dx} \quad (14)$$

Substitute Eqs. 13 and 14 into Eq. 12. Combine the result with the differentiation of Eq. 9 and simplify it to obtain the following equation:

$$\frac{d^4 f}{dx^4} + A_1 \cdot f + A_2 \cdot \frac{d^2 T}{dx^2} = 0 \quad (15)$$

where $A_1 = \frac{K_v}{e} \cdot \left(\frac{1}{E_c \cdot I_c} + \frac{1}{E_w \cdot I_w} \right)$; $A_2 = \frac{K_v}{e} \cdot \left(\frac{h_c}{2E_c \cdot I_c} - \frac{h_w}{2E_w \cdot I_w} \right)$.

The following equation can be obtained from assumptions (2):

$$e \cdot q = K_1 \cdot S \quad (16)$$

Substituting Eqs. 9 and 6 into Eq. 16 yields the following:

$$\frac{d^2 T}{dx^2} = \frac{K_1}{e} (\varepsilon_w - \varepsilon_c) \quad (17)$$

Using the basic calculation assumption (3), set the cross-sectional area of the concrete slab and the timber beam to A_c and A_w . According to the correlation between the internal force and strain, Eqs. 18 and 19 are as follows:

$$\varepsilon_c = \frac{M_c}{E_c \cdot I_c} \cdot \frac{h_c}{2} - \frac{T}{E_c \cdot A_c} \quad (18)$$

$$\varepsilon_w = \frac{T}{E_w \cdot A_w} - \frac{M_w}{E_w \cdot I_w} \cdot \frac{h_w}{2} \quad (19)$$

Substitute Eqs. 18 and 19 into Eq. 17 to obtain the following equation:

$$\frac{d^2 T}{dx^2} = \frac{K_1}{e} \cdot \left(\frac{1}{E_c \cdot A_c} + \frac{1}{E_w \cdot A_w} \right) \cdot T - \frac{K_1}{e} \cdot \left(\frac{M_w}{E_w \cdot I_w} \cdot \frac{h_w}{2} + \frac{M_c}{E_c \cdot I_c} \cdot \frac{h_c}{2} \right) \quad (20)$$

Applying internal and external bending moment balance conditions yields the following:

$$M_w + M_c = M - T \cdot h \quad (21)$$

Solve Eqs. 10, 11, and 21 simultaneously to obtain the following equations:

$$\frac{M_c}{E_c I_c} = \frac{E_w I_w e}{(E_c I_c + E_w I_w) K_v} \cdot \frac{d^2 f}{dx^2} + \frac{M - T \cdot h}{E_c I_c + E_w I_w} \quad (22)$$

$$\frac{M_w}{E_w I_w} = -\frac{E_c I_c e}{(E_c I_c + E_w I_w) K_v} \cdot \frac{d^2 f}{dx^2} + \frac{M - T \cdot h}{E_c I_c + E_w I_w} \quad (23)$$

Substitute Eqs. 22 and 23 into Eq. 20 and simplify to obtain the following:

$$\frac{d^2 T}{dx^2} - C_1 \cdot T + C_2 \cdot \frac{d^2 f}{dx^2} + C_3 \cdot M = 0 \quad (24)$$

where $C_1 = \frac{K_1}{e} \cdot \left(\frac{1}{E_c A_c} + \frac{1}{E_w A_w} + \frac{h^2}{E_c I_c + E_w I_w} \right)$; $C_2 = \frac{K_1}{K_v} \cdot \frac{-E_c I_c h_w + E_w I_w h_c}{2(E_c I_c + E_w I_w)}$; $C_3 = \frac{K_1}{P} \cdot \frac{h}{E_c I_c + E_w I_w}$. Eq. 24 is the differential equation set for axial force T and vertical-uplift force per unit length f .

Solving the Differential Equation

Rewrite Eq. 24 to obtain the following:

$$\frac{d^2 f}{dx^2} = -\frac{1}{C_2} \cdot \frac{d^2 T}{dx^2} + \frac{C_1}{C_2} \cdot T - \frac{C_3}{C_2} \cdot M \quad (25)$$

Differentiate Eq. 25 twice to obtain the following:

$$\frac{d^4 f}{dx^4} = -\frac{1}{C_2} \cdot \frac{d^4 T}{dx^4} + \frac{C_1}{C_2} \cdot \frac{d^2 T}{dx^2} - \frac{C_3}{C_2} \cdot \frac{d^2 M}{dx^2} \quad (26)$$

Integrate Eq. 25 twice to obtain the following:

$$f = -\frac{T}{C_2} + \frac{C_1}{C_2} \cdot \int (\int T dx) dx - \frac{C_3}{C_2} \cdot \int (\int M dx) dx + t_1 \cdot x + t_2 \quad (27)$$

The quantities t_1 and t_2 are integration constants. Substituting Eqs. 26 and 27 into Eq. 15 yields the following:

$$\frac{d^4 T}{dx^4} - (C_1 + A_2 \cdot C_2) \cdot \frac{d^2 T}{dx^2} + A_1 \cdot T - A_1 \cdot C_1 \cdot \int (\int T dx) dx + C_3 \cdot \frac{d^2 M}{dx^2} \cdot A_1 \cdot C_1 \cdot \int (\int M dx) dx - A_1 \cdot C_2 \cdot t_1 \cdot x - A_1 \cdot C_2 \cdot t_2 = 0 \quad (28)$$

Differentiate the above equation twice, and apply $\frac{d^4 M}{dx^4} = 0$ to obtain the following:

$$\frac{d^6 T}{dx^6} - (C_1 + A_2 \cdot C_2) \cdot \frac{d^4 T}{dx^4} + A_1 \cdot \frac{d^2 T}{dx^2} - A_1 \cdot C_1 \cdot T = -A_1 \cdot C_3 \cdot M \quad (29)$$

Substitute Eq. 26 into Eq. 15 to obtain the following:

$$f = \frac{1}{A_1 \cdot C_2} \cdot \frac{d^4 T}{dx^4} - \left(\frac{A_2}{A_1} + \frac{C_1}{A_1 \cdot C_2} \right) \cdot \frac{d^2 T}{dx^2} + \frac{C_3}{A_1 \cdot C_2} \cdot \frac{d^2 M}{dx^2} \quad (30)$$

Equation 29 is an inhomogeneous linear differential equation for the axial force $T(x)$. According to the boundary conditions of the simply supported composite beam, which are listed in the Eqs. 38 through 41, the differential Eq. 29 will be solved and the expression to calculate the axial force $T(x)$ will be obtained. The expression of the uplift force is obtained by substituting $T(x)$ into Eq. 30. The general solution of the differential Eq. 29 consists of the corresponding homogeneous solution of the homogeneous

differential equation $T_q(x)$ and the particular solution of the inhomogeneous differential equation $T_p(x)$ as follows:

$$T(x) = T_q(x) + T_p(x) \quad (31)$$

Finding the General Solution $T_q(x)$

The homogeneous differential equation corresponding to the sixth-order linear inhomogeneous differential Eq. 28 is as follows:

$$\frac{d^6 T_q(x)}{dx^6} - (C_1 + A_2 \cdot C_2) \cdot \frac{d^4 T_q(x)}{dx^4} + A_1 \cdot \frac{d^2 T_q(x)}{dx^2} - A_1 \cdot C_1 \cdot T_q(x) = 0 \quad (32)$$

The above equation has two real roots opposite to each other and two pairs of conjugate complex roots. The general solution can be written as follows:

$$T_q(x) = B_1 \cdot \text{sh}R_1 x + B_2 \cdot \text{ch}R_1 x + \cos\beta x \cdot (B_3 \cdot \text{sh}\alpha x + B_4 \cdot \text{ch}\alpha x) + \sin\beta x \cdot (B_5 \cdot \text{sh}\alpha x + B_6 \cdot \text{ch}\alpha x) \quad (33)$$

where R_1 is a positive real root of the corresponding characteristic equation of Eq. 29, α and β are the real and imaginary parts of the two pairs of conjugate complex roots of the corresponding characteristic equation of Eq. 25, and the coefficients B_1 - B_6 are hypothetical coefficients.

Finding the Particular Solution $T_p(x)$

The composite beam bending moment calculated from Fig. 7 is as follows:

$$\left\{ \begin{array}{l} \text{Pure bending segment: } M(x) = P \cdot \left(\frac{L}{2} - b\right); \quad (-b \leq x \leq b) \\ \text{Bend - shear segment: } \left\{ \begin{array}{l} M(x) = P \cdot \left(\frac{L}{2} - x\right); \quad (x > b) \\ M(x) = P \cdot \left(\frac{L}{2} + x\right); \quad (x < -b) \end{array} \right. \end{array} \right. \quad (34)$$

Let the particular solution of the axial force $T(x)$ differential equation be as follows:

$$\left\{ \begin{array}{l} \text{Pure bending segment: } T_p(x) = g_0; \\ \text{Bend - shear segment: } T_p(x) = g_0 + g_1 \cdot x; \end{array} \right. \quad (35)$$

Substituting Eqs. 34 and 35 into Eq. 29 yields the following constant coefficients:

$$\left\{ \begin{array}{l} \text{Pure bending segment: } g_0 = C_3 \cdot P \cdot \frac{L-2b}{2C_1}; \\ \text{Bend - shear segment: } \left\{ \begin{array}{l} g_0 = C_3 \cdot P \cdot L/2C_1; \\ g_1 = -C_3 \cdot \frac{P}{C_1}; \end{array} \right. \end{array} \right. \quad (36)$$

By substituting Eq. 36 into Eq. 35, the particular solution of the inhomogeneous linear differential equation of the axial force $T(x)$ is as follows:

$$\left\{ \begin{array}{l} \text{Pure bending segment: } T_p(x) = C_3 \cdot P \cdot \frac{L-b}{C_1}; \quad (-b \leq x \leq b) \\ \text{Bend - shear segment: } \left\{ \begin{array}{l} T_p(x) = C_3 \cdot P \cdot \frac{L}{2C_1} - C_3 \cdot P \cdot \frac{x}{C_1}; \quad (x > b) \\ T_p(x) = C_3 \cdot P \cdot \frac{L}{2C_1} + C_3 \cdot P \cdot \frac{x}{C_1}; \quad (x < -b) \end{array} \right. \end{array} \right. \quad (37)$$

Finding the Complete Solution $T(x)$

Coefficients B_1 - B_6 must be estimated to obtain the general solution $T(x)$ by solving Eqs. 31, 33, and 37. These coefficients can be obtained from the six equations listed in the boundary conditions of the simply supported timber-concrete composite beam as follows:

(1) The axial force T of the concrete slab and the timber beam at the beam end of the simple-supported composite beam is zero as follows:

$$T|_{x=\pm L/2} = 0 \quad (38)$$

(2) Under the action of a symmetrical concentrated load, and because of the symmetry of the force of the simply supported timber-concrete composite beam, the relative horizontal slip at the midspan cross-section is zero as follows:

$$\frac{dT}{dx}|_{x=0} = 0 \quad (39)$$

(3) The slab and the timber beam of the simply supported timber-concrete composite beam have zero slip strain at the beam end as follows:

$$\frac{d^2T}{dx^2}|_{x=\pm \frac{L}{2}} = 0 \quad (40)$$

(4) The total bending moment of a timber-concrete composite beam (M) has two components (Jiang *et al.* 2007), the overall bending moment (M_a), and the local bending moment (M_l). M_a acts on the entire composite beam. Under M_a , the timber beam and the concrete slab are fully integrated, and there is no relative horizontal slip or vertical uplift displacement at the beam-slab interface. Within this scenario, the timber beam and the concrete slab function as a single object. Under M_l , the composite beam is equivalent to a timber beam and a concrete slab. M_l is composed of the bending moment acting only on the timber beam (M_{lw}) and the bending moment acting only on the concrete slab (M_{lc}). Within this scenario, relative horizontal slip and vertical uplift displacement may occur at the interface between the timber beam and the concrete slab. Therefore, the following equation is obtained:

$$M = M_a + M_l = M_a + M_{lc} + M_{lw} \quad (41)$$

Under a load, the timber beam and the concrete slab have similar bending curvatures at the elastic stage because of the small uplift displacement between the beam and the slab. The bending curvature of the timber beam can then be considered to be the same as that of the concrete slab. Therefore, the following equation is obtained:

$$\frac{M_{lc}}{E_w I_c / \alpha_E} = \frac{M_{lw}}{E_w I_w} \quad (42)$$

where α_E is the ratio of the elastic modulus of the timber to that of the concrete.

Under M_l , the slip strain of the composite beam (ε) is the sum of the tensile strain at the lower edge of the concrete slab (ε_{lc}) and the compressive strain at the upper edge of the timber beam (ε_{lw}) at the interface:

$$\varepsilon = \varepsilon_{lc} + \varepsilon_{lw} \quad (43)$$

where ε_{lc} satisfies the following equation,

$$\varepsilon_{lc} = \frac{M_{lc}}{E_w I_c / \alpha_E} \cdot \frac{h_c}{2} \quad (44)$$

and ε_{lw} satisfies the following equation:

$$\varepsilon_{1w} = \frac{M_{1w}}{E_w I_w} \cdot \frac{h_w}{2} \quad (45)$$

Therefore, ε can be expressed as follows:

$$\varepsilon = 2h \cdot \Delta\varphi = 2h \cdot \frac{\zeta \cdot M}{E_w \cdot I} \quad (46)$$

Equation 47 is obtained by substituting Eqs. 44, 45, and 46 into Eq. 43:

$$\frac{M_{1c}}{E_w I_c / \alpha_E} \cdot \frac{h_c}{2} + \frac{M_{1w}}{E_w I_w} \cdot \frac{h_w}{2} = 2h \cdot \frac{\zeta \cdot M}{E_w \cdot I} \quad (47)$$

where $\Delta\varphi$ is the curvature of the cross-section of the composite beam caused by the relative slip at the interface between the timber beam and the concrete slab, I is the conversion of the moment of inertia of the cross-section of the composite beam, $E_w I$ is the converted bending stiffness of the cross-section of the composite beam, and ζ is the composite beam stiffness reduction factor, which is calculated according to the literature (Xu and Chen 2013).

Equation 48 is obtained by substituting Eq. 42 into Eq. 47:

$$\frac{M_{1w}}{E_w I_w} \cdot \frac{h_c}{2} + \frac{M_{1w}}{E_w I_w} \cdot \frac{h_w}{2} = 2h \cdot \frac{\zeta \cdot M}{E_w \cdot I} \quad (48)$$

The following equation is obtained from Fig. 10:

$$\frac{h_w}{2} + \frac{h_c}{2} = h \quad (49)$$

The equation for M_{1w} is obtained by substituting Eq. 49 into Eq. 48:

$$M_{1w} = \frac{2I_s}{I} \cdot \zeta \cdot M \quad (50)$$

Considering the M_{1w} results from the local load acting only on the timber beam, an equilibrium equation for the boundary conditions of the vertical-uplift force can be obtained:

$$\int_{-L/2}^{L/2} f \cdot dx = \frac{2I_w}{I} \cdot \zeta \cdot 2P \quad (51)$$

The values of B_1 to B_6 can be obtained using Eqs. 38 to 51. It is found that $B_1=B_3=B_6=0$, yields the general solution of the differential Eq. 29 as follows:

$$T(x) = B_2 \cdot \operatorname{ch} R_1 x + B_4 \cdot \cos \beta x \cdot \operatorname{ch} \alpha x + B_5 \cdot \sin \beta x \cdot \operatorname{sh} \alpha x + T_p(x) \quad (52)$$

Substituting the result of Eq. 52 into Eq. 30, the equation for calculating the uplift force per unit length at the interlayer of a composite beam is as follows:

$$f = D_1 \cdot \operatorname{ch}(R_1 \cdot x) + D_2 \cdot \cos(\beta \cdot x) \cdot \operatorname{ch}(\alpha \cdot x) + D_3 \cdot \sin(\beta \cdot x) \cdot \operatorname{sh}(\alpha \cdot x) \quad (53)$$

where $C_0 = C_1 + A_2 \cdot C_2$;

$$D_1 = R_1^2 \cdot B_2 \cdot (R_1^2 - C_0) / (A_1 \cdot C_2);$$

$$D_2 = [\alpha^4 + \beta^4 - 6\alpha^2 \cdot \beta^2 - C_0 \cdot (\alpha^2 - \beta^2)] \cdot B_4 / (A_1 \cdot C_2) + 2\alpha \cdot \beta \cdot [2(\alpha^2 - \beta^2) - C_0] \cdot B_5 / (A_1 \cdot C_2);$$

$$D_3 = [\alpha^4 + \beta^4 - 6\alpha^2 \cdot \beta^2 - C_0 \cdot (\alpha^2 - \beta^2)] \cdot B_5 / (A_1 \cdot C_2) - 2\alpha \cdot \beta \cdot [2(\alpha^2 - \beta^2) - C_0] \cdot B_4 / (A_1 \cdot C_2).$$

RESULTS AND DISCUSSION

When the concentrated loads are 16 kN, 28 kN, 40 kN, 70 kN, and 100 kN, the theoretical values of the uplift force on the bolts at the ends of beams CWW1 to CWW5 are compared with the experimental values (Fig. 11). The experimental values of the uplift force are obtained by substituting the measured vertical strain of the bolt at the beam end (Table 3) into Eq. 1.

Table 3. Experimental Vertical Strain of Bolt at the End of Beam

Load (kN)	Experimental vertical strain of bolt ($\mu\epsilon$)				
	CWW1	CWW2	CWW3	CWW4	CWW5
0	0	0	0	0	0
16	85	107	126	128	95
28	154	201	249	256	185
40	225	296	369	405	268
70	410	559	682	814	500
100	593	891	1089	1255	805

The comparison leads to the following conclusions:

(1) As the load increases, the uplift force on the bolt at the end of the beam also increases. The curves show that the relationship between load and uplift force is almost linear in the elastic stage.

(2) The spacing between adjacent bolt shear connectors, *i.e.*, the shear connection ratios of shear connection, has a significant influence on the uplift force on the beam end. The uplift force on the beam end increases as the bolt spacing increases. Both the calculated and measured results show that as the bolt spacing increases, the uplift force on a single bolt increases.

(3) The shear connection ratios of shear connectors of beams CWW2 and CWW5 are the same, even though the arrangements of the bolts are different. Under the same load, the uplift force on the end of beam CWW5 is slightly less, indicating that the bolt placement in beam CWW5 is better under the two-point loading mode.

(4) As the shear connection ratios of shear connectors decreases, the stiffness of composite beam changes because of the cracking of the concrete flange and the timber beam. However, the stiffness is constant in the theoretical calculation, which causes the theoretical value to deviate from the experimental value.

(5) Table 4 compares the mean, standard deviation and coefficient of variance between the calculated and test results of the uplift force on the bolts at the ends of beams CWW1 to CWW5. The mean value for five beams increases as the shear connection ratios of connection decreases, indicating an increase in the deviation of the theoretical values from the experimental values. The standard deviation and coefficient of variance of the five beams also increase as the shear connection ratios of the connectors decreases, indicating increased fluctuations in the deviation of the theoretical values from the experimental values and an increase in the data dispersion.

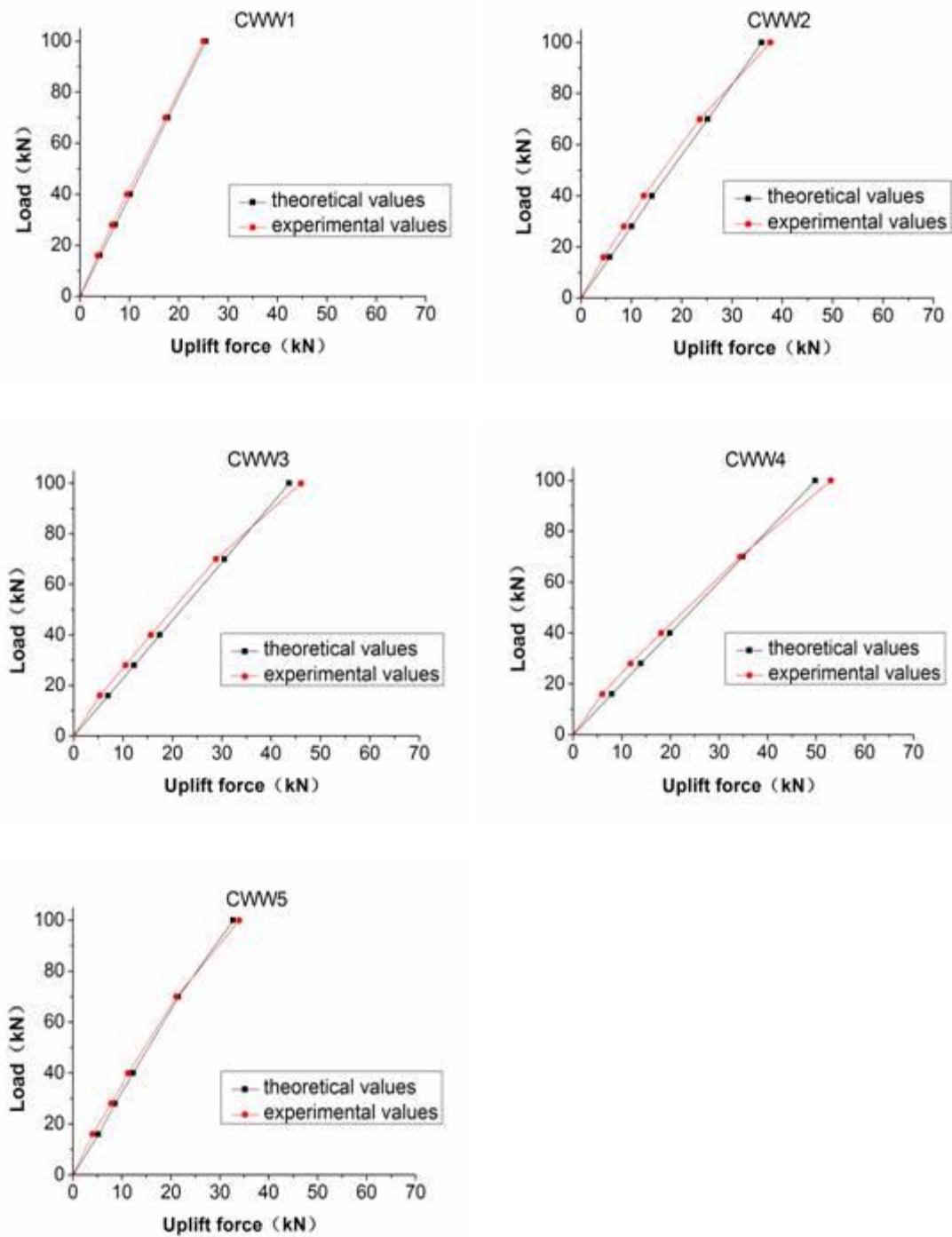


Fig. 11. Comparison of the theoretical and experimental values of the uplift force on the bolts at the ends of the TCC beams

Table 4. Comparison of Theoretical and Experimental Value

NO. of beam	CWW1	CWW2	CWW3	CWW4	CWW5
average value	1.07	1.12	1.12	1.18	1.10
standard deviation	0.04	0.11	0.12	0.19	0.11
coefficient of variation	0.04	0.10	0.11	0.16	0.10

CONCLUSIONS

1. A theoretical calculation method for the vertical-uplift force along the interlayer of the TCC beam is proposed. Under a concentrated load, the elastic theory was used to establish the differential equations for the TCC beams with respect to the axial force and the vertical-uplift force.
2. Tests showed that the shear connection ratios of shear connection were directly proportional to the uplift force. The calculated uplift forces on the bolts are in good agree with the test results, which provides a theoretical basis for the anti-uplift design of bolts.
3. In general, the theoretical calculation of the TCC composite beam simultaneously considers that the influence of interlayer slip and vertical uplift has significance, which is more correct theoretical and has higher practical value than the existing analytic methods that ignore the influence of uplift.

ACKNOWLEDGMENTS

The authors are grateful for the support of the Hunan Provincial Engineering Laboratory Open Fund for Manufacturing and Application Technologies of Modern Timber Structure Engineering Materials(Project No.HELFMTS1706), the Hunan Provincial Department of Education Scientific Research Project(Project No.198014030).

REFERENCES CITED

- Ayoub, A. (2001). "A two-fold mixed variational principle for partially connected composite beams," *Finite Elements in Analysis and Design* 37(11), 929-959. DOI: 10.1016/s0168-874x(01)00076-2
- Ayoub, A. (2005). "A force-based model for composite steel-concrete beams with partial interaction," *Journal of Constructional Steel Research* 61(3), 387-414. DOI: 10.1016/j.jcsr.2004.08.004
- BS5400-5. (2005). "Steel, concrete and composite bridges – Part 5: Code of practice for design of composite bridges," British Standards Institution, London, UK.
- Cas, B., Saje, M., and Planinc, I. (2004). "Non-linear finite element analysis of composite planar frames with an interlayer slip," *Computers & Structures* 82 (23–26), 1901-1912. DOI: 10.1016/j.compstruc.2004.03.070
- Cas, B., Planinc, I., and Schnabl, S. (2018). "Analytical solution of three-dimensional two-layer

- composite beam with interlayer slips,” *Engineering Structures* 173(10), 269-282. DOI: 10.1016/j.engstruct.2018.06.108
- Dias, A. M. P. G., and Jorge, L. F. C. (2011). “The effect of ductile connectors on the behaviour of timber concrete composite beams,” *Engineering Structures* 33(11), 3033-3042. DOI: 10.1016/j.engstruct.2011.05.014
- Dias, A. M. P. G. (2012). “Analysis of the nonlinear behavior of timber-concrete connections,” *Journal of Structural Engineering* 138(9), 1128-1137. DOI:10.1061/(Asce)St.1943-541x.0000523
- Dias, A. M. P. G., Martins, A. R. D., Simões, L. M. C., Providência, P. M., and Andrade, A. A. M. (2015). “Statistical analysis of timber-concrete connections – Mechanical properties,” *Computers & Structures* 155(4), 67-84. DOI: 10.1016/j.compstruc.2015.02.036
- EN 1995-2 (2004). “Eurocode 5: Design of timber structures – Part 2: Bridges,” European Committee for Standardization, Brussels, Belgium.
- Fu, G., Zhao, H. Y., Xue, J., Y., and Xiong, H. C. (2008). “The theoretical research on uplift of the steel- concrete composite beam,” *Journal of Xi’An University of Architecture & Technology* 40(3), 335-339. DOI: 10.3969/j.issn.1006-7930.2008.03.008
- Gara, F., Ranzi, G., and Leoni, G. (2006). “Displacement-based formulations for composite beams with longitudinal slip and vertical uplift,” *International Journal for Numerical Methods in Engineering* 65(8), 1197-1220. DOI: 10.1002/nme.1484
- GB/T 1938-2009. (2009). “Method of testing in tensile strength parallel to grain of wood,” Chinese Ministry of Construction, Beijing, China.
- GB/T 1935-2009. (2009). “Method of testing in compressive strength parallel to grain of wood,” Chinese Ministry of Construction, Beijing, China.
- Gutkowski, R., Brown, K., Shigidi, A., and Natterer, J. (2008). “Laboratory tests of composite wood-concrete beams,” *Construction and Building Materials* 22(6), 1059-1066. DOI: 10.1016/j.conbuildmat.2007.03.013
- He, G. J., Xie, L., Wang, A., Yi, J., Peng, L. N., Chen, Z. A., Gustafsson, P. J., and Crocetti, R. (2016). “Shear behavior study on timber-concrete composite structure with bolts,” *BioResources* 11(4), 9205-9218. DOI: 10.15376/biores.11.4.9205-9218
- Jiang, X. G., Ju, J. S., and Fu., X. R. (2007). “Analysis of elastic stress of composite steel-concrete beams considering slip effect,” *Engineering Mechanics* 24(1), 143-146. DOI: 10.3969/j.issn.1000-4750.2007.01.024
- Jorge, L. F., J. Schanzlin, S. M. R., Lopes, H., Cruz, U., and Kuhlmann. (2010). “Time-dependent behaviour of timber lightweight concrete composite floors,” *Engineering Structures* 32(12), 3966-3973. DOI: 10.1016/j.engstruct.2010.09.007
- Lopes, S., Jorge, L., and Cruz, H. (2012). “Evaluation of non-linear behavior of timber-concrete composite structures using FE model,” *Materials and Structures* 45(1), 653-662. DOI: 10.1617/s11527-011-9787-9
- Martins, C., Dias, A. M. P. G., Costa, R., and Santos, P. (2016). “Environmentally friendly high performance timber-concrete panel,” *Construction and Building Materials* 102, Part 2: 1060-1069. DOI: 10.1016/j.conbuildmat.2015.07.194
- Ranzi, G., Bradford, M. A., and Uy, B. A. (2004). “Direct stiffness analysis of a composite beam with partial interaction,” *International Journal for Numerical Methods in Engineering* 61(5), 657-672. DOI: 10.1002/nme.1091
- Rodrigues, J. N., Dias, A. M. P. G., and Providência, P. (2013). “Timber-concrete composite bridges: State-of-the-art review,” *BioResources* 8(4), 6630-6649. DOI: 10.15376/biores.8.4.6630-6649
- Xie, L., He, G. J., Wang, A., Gustafsson, P. J., Crocetti, R., Chen, L. P., Li, L., and Xi, W. H.

- (2017). “Shear capacity of stud-groove connector in glulam-concrete composite structure,” *BioResources* 12(3), 4690-4706. DOI: 10.15376/biores.12.3.4960-4706
- Xu, R. Q., and Chen, D. Q. (2013). “Modified reduced stiffness method for calculating the deflection of composite beams,” *Engineering Mechanics*. 30(2), 285-291. DOI: 10.6052/j.issn.1000-4750.2011.08.0557
- Yeho, D., Fragiaco, M., de Franceschi, M., and Boon, K. H. (2011). “State of the art on timber-concrete composite structures: Literature review,” *Journal of Structural Engineering* 137(10), 1085-1095. DOI: 10.1061/(ASCE)ST.1943-541X.0000353

Article submitted: October 31, 2019; Peer review completed: January 15, 2020; Revised version received and accepted: June 29, 2020; Published: July 29, 2020.

DOI: 10.15376/biores.15.3.7079-7099